One-Pot Synthesis of Ag/Fe$_3$O$_4$ Nanocomposite: Preparation and Characterization

Babak Sadeghi*

Department of Chemistry, Tonekabon Branch, Islamic Azad University, Tonekabon, Iran

ARTICLE INFO	ABSTRACT

In this study, Ag/Fe$_3$O$_4$ nanocomposite (AFN) was synthesized by using a simple chemical reduction based method. The size and shape of AFN was controlled by using condensation (Fe$_2$O$_3$ (2.975 mmol), NaBH$_4$ (21.25 mmol), AgNO$_3$ (2.532 mmol), and polyvinylpyrrolidone (PVP) (8.925 mmol K30 Mr=10.000)) at 40°C. The synthesized AFN was characterized by X-ray diffraction analysis (XRD), scanning electron microscopy (SEM), transmission electron microscopy (TEM) and electron diffraction X-ray spectroscopy (EDS). The XRD Measurements confirmed that Ag/Fe$_3$O$_4$ nanocomposite has the crystalline structure. The SEM images of the as-deposited Ag/Fe$_3$O$_4$ nanocomposite (AFN) demonstrated that the particles aggregate into an organized spherical structure, which is characterized by a diameter of 10-20 nm. This type of porous aggregate is characterized by large surface area, which could have potential applications in the areas of catalysis and filtration. The population distribution as measured from the TEM images shows that the average particle size for AFN is 10-20 nm.

1-Introduction

Powder metallurgy allows processing of oxide dispersion strengthened alloys with unique microstructures by milling of powders to small sizes with the addition of yttrium oxide. Widespread applications of powder metallurgy may be found in aerospace, plastics, printing, catalysis, coatings, agri- culture, magnetism and several other industrial and technological areas [1-5].

 Several examples of nanocrystalline systems where the Hall–Petch (HP) relationship has been demonstrated include Cu, Al, Ni, Ti, Fe, Cr, TiO$_2$, FeAl and NbAl$_3$ [6-14]. In the case of Cu, the yield strength for a nanocrystalline powder with an average size of 20 nm particles [1, 15]. For intermetallic materials such as FeAl, nanostructured compacts were reported to have iron alloys [16]. A 3-fold increase in the

Vickers hardness was reported for ball milled Fe- 45% Al samples [13].

Intermetallic materials based on iron aluminides are an important class of materials due to a combination of their high tensile strengths and low densities. They also possess excellent oxidation and corrosion resistances at high temperatures. In addition, they are resistant to sulfidiation in H$_2$S and SO$_2$ [17-19]. These materials are excellent candidates for potential applications as thermal structures, heating elements, and exhaust manifolds for automobiles [20-22]. Several of such applications are impeded due to the low room temperature ductility, low strength at high temperatures, and the severe embrittlement of the bulk materials in air due to reaction with water vapor [23]. These difficulties have been recently overcome through the development of

---

* Corresponding author:
E-mail address: bsadeghi1177@gmail.com

a novel roll compaction technique based on thermochemical processing [24, 25]. Fully dense fine-grained sheets of 0.20 mm thickness with excellent yield strength, ultimate tensile strength and tensile elongation could be produced by this method. However, in order to produce thinner sheets and foils of FeAl that are required in many other applications, powders of nano- sized particles need to be used as the starting material instead of the micron sized powders employed in the above mentioned investigations.

A variety of physical and chemical methods have been employed to synthesize nanopowders of semiconductors, metals, oxides and rare earth metals [26–30]. However, very little progress has been made in synthesizing nanosized multicomponent crystallites due to the difficulty in controlling the composition of nanomaterials.

The most common physical method used to synthesize intermetallic nanostructured materials is mechanical alloying or ball milling [31–33]. Ball milling is associated with long periods of milling times in order to obtain crystallite sizes below 20 nm. In addition, contamination from the atmosphere and the milling media is common in ball milling [34].

Intermetallic nanoparticles have been prepared by chemical methods such as reduction reactions [35, 36]. For example, TiAl and $TiAl_3$ have been prepared by the reduction of $TiCl_3$ with lithium aluminum hydride [37]. Bonnemann has prepared a wide variety of binary alloy nanoparticles by the co-reduction of two metal halides in the presence of hydrotriorganoborates such as $LiBEt_3H$ and $NaBEt_3H$ [38]. In another approach, Sohn and his colleagues reduced mixtures of metal chlorides in the vapor phase either with hydrogen or magnesium vapor to produce ultrafine intermetallic powders [39, 40]. Evaporation methods have been effectively used by researchers to prepare significant quantities of metallic nanoparticles [41, 42]. Thermal evaporation has not been very successful for multicomponent systems since one of the metallic elements typically evaporates before the other due to the difference in vapor pressures of the evaporating metals. Haubold et al. used a flash evaporation approach in which they continuously filled small amounts of NiAl powders into a resistance heated crucible and evaporated directly to form nanosized Ni_3Al [43]. Magnetron sputtering which is advantageous to use for metals and alloys with high melting points has also been used to synthesize intermetallic nanoparticles [44].

We have recently developed a reduction method of converting Ag nanospheres into nanorods [45], nanoplates [46], their antibacterial activity [47, 48], an improved easy synthetic route for silver nanoparticles in poly (diallyldimethylammonium chloride) (PDDA) [49], synthesis of gold/HPC (HydroxyPropyl Cellulose) hybrid nanocomposite [50], preparation of ZnO/Ag nanocomposite [51] and comparison nanosilver particles and nanosilver plates for the oxidation of ascorbic acid [52]. Regarding the role of green chemistry, we successfully demonstrated that the size, shape and the antibacterial activity of silver and gold nanoparticles by the reduction of silver and gold ions with bioreductants and green chemistry methods [53-57]. The long-term objective of the present work is to optimize the size, composition and surface morphology of the Ag/Fe_3O_4 nanocomposite (AFN) in such a way as to enhance both the mechanical and magnetic properties of the nanoparticle assemblies. In this study, Ag/Fe_3O_4 nanocomposite (AFN) has been synthesized by using a simple chemical reduction based method in which no $FeCl_3.H_2O$ was added to the reaction system. This may lead to a novel form of advanced material based on consolidated nanoparticles, and combine high electrical resistivity, oxidation resistance, ductility and unique magnetic properties.

2- Experimental
2-1-Synthesis of Ag/Fe_3O_4 nanocomposite
In this work, the synthesis of Ag/Fe_3O_4 nanocomposite (AFN) involves the use of chemical reduction method and controlled condensation of Fe_2O_3 (2.975 mmol), $NaBH_4$ (21.25 mmol), $AgNO_3$ (2.532 mmol) and polyvinylpyrrolidone (PVP) (8.925 mmol K30, Mr = 10 000) at 40°C. The autoclave was allowed to cool down to room temperature. Finally, the reaction product was collected and washed thoroughly with distilled water and absolute ethanol, followed by drying under vacuum at room temperature.

2-2-Synthesis of Ag nanoparticles for catalysis comparison

The synthesis process was the same as that for the Ag/Fe$_3$O$_4$ nanocomposite (AFN) except that no Fe$_2$O$_3$ was added to the reaction system. The final product was obtained by centrifugation and washed with acetone and ethanol, and then dried under vacuum at room temperature. The formed nanoparticles were metallic silver as confirmed by SEM images.

2-3-Synthesis of Fe$_3$O$_4$ nanoparticles for catalysis comparison

The synthesis process was the same as that for the AFN, except that no AgNO$_3$ was added to the reaction system. The formed nanoparticles were magnetite as confirmed by SEM images.

2-4-Catalytic testing

In a typical catalytic reaction, 6 mL of aqueous 4-Nitrophenol (4-NP) solution (0.2 mM) and 1.0 mL of aqueous NaBH$_4$ (30 mM) solution were mixed together in a standard quartz cell, having 1 cm path length and then 1 mL of aqueous Ag/Fe$_3$O$_4$ nanocomposite (AFN) (0.5 mg mL^{-1}) was added to the reaction mixture under constant magnetic stirring. Immediately after that, the solution was transferred to a standard quartz cell, and the UV-vis absorption spectra were recorded with a time interval of 2 min in a scanning range of 200-800 nm at ambient temperature. After completion of the reaction, the catalyst was recovered by centrifugation. The precipitate was repeatedly washed with deionized water in consecutive washing cycles. Ultrasonic treatment was used in every cycle in order to re-disperse the catalyst and remove the adsorbed impurities. After washing, the catalyst was directly used for recycling test. After each recycle, the centrifuge supernatant was collected and detected by atomic absorption spectroscopy to determine the content of Ag/Fe$_3$O$_4$ nanocomposite (AFN). The reduction of 4-nitrophenol and 4-nitroaniline was also investigated under the same conditions.

2-5-Characterization

The XRD patterns were obtained by using the Philips X'Pert Materials Research Diffractometer, which uses the Cu-Kα radiation. The particle size and shape were investigated using a Jeol JEM-200FXII transmission electron microscope (TEM) operated at 200 kV. The coated samples were observed by using scanning electron microscopy (SEM, LEO 440i) at the accelerating voltage of 10 kV.

3-Results and discussion

3-1-Characterization of the Ag/Fe$_3$O$_4$ nanocomposite (AFN) by X-ray diffraction method

The XRD pattern of the Ag nanoparticles shows the peaks which, upon comparison with the known bulk data, can be assigned to reflections from the 111, 200, 220 and 311 planes of Ag Fig.1a. The XRD pattern of the Fe nanopowders shows three strong lines assigned to the reflections from the 110, 200 and 211 planes at the scattering angles of 44.65, 65.01 and 82.33, respectively (Fig.1b). The lattice parameters for the unit cells of AFN samples were calculated assuming cubic symmetry in both cases. The calculated lattice parameters for Ag and Fe are 4.0504 and 2.8666, respectively, which are in good agreement with the known lattice parameters for bulk Ag and bulk Fe (4.0494 and 2.8664), respectively [58].

The crystallinity of the Ag/Fe$_3$O$_4$ nanocomposite (AFN) is verified in Fig.1c, which displays the XRD pattern for the AFN obtained following vaporization of a bulk Fe – 40 at % Ag target. It is evident that the XRD pattern matches neither with Ag nor with Fe. The strong diffraction peaks at the scattering angles of 30.76, 44.16, 64.21, 81.26 and 97.48 can be assigned to scattering from the 100, 110, 200, 211 and 220 planes, respectively, of the AFN crystal lattice.

The calculated lattice parameter (2.8984) of AFN is in good agreement with the bulk lattice parameter (2.8954) [58]. The crystallinity of the Ag/Fe$_3$O$_4$ micronized (AFM) is showed in Fig.1d.

A comparison of the XRD data of the micron sized (Fig.1d) and the nanosized AFN (Fig.1c) reveals a significant decrease in the intensity of the 100 peak, which is a superlattice reflection, in the nanosized sample.
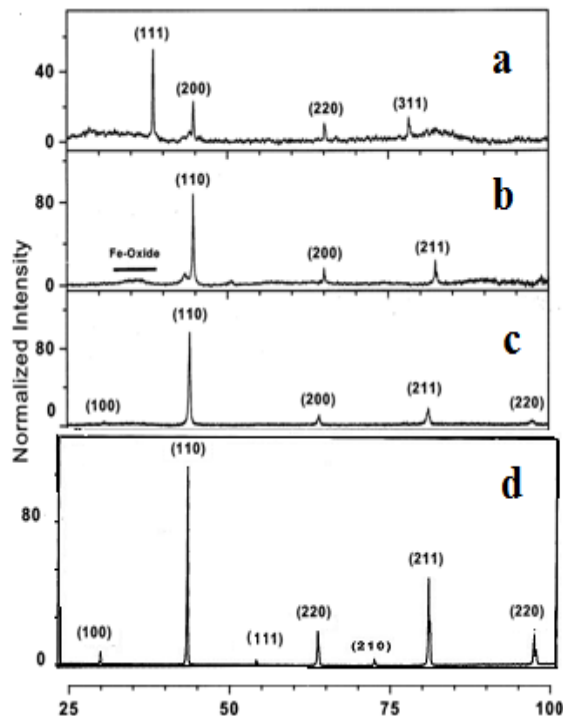
Fig.1. XRD patterns of the nanopowders of (a) Ag, (b) Fe (c) XRD pattern of the Ag/Fe$_3$O$_4$ nanocomposite (AFM) and (d) XRD pattern of the Ag/Fe$_3$O$_4$ micronized (AFM), respectively.

This decrease in intensity indicates a decrease in the long-range order within the nanoparticle sample.

As suggested by Bakker et al. [59], the relative long range order parameter (*S*) can be determined by comparing the superlattice to fundamental [100/110] peak ratio in the nanopowders sample to a reference bulk sample. In this result, the growth of sample is along 100 for one shape and along 110 for the other shape. For a long-range ordered system (*S* value), it is usually possible to define sublattices. Consider a B$_2$ structure. One of the simple-cubic lattice type sublattices is occupied by A-type atoms, the other by B-type atoms. For perfect order and perfect stoichiometry, you get a long-range order parameter equal to one. If, on the other hand, the two sublattices are occupied

by 50% A-type and 50% B-type atoms each, you get a long-range order parameter equal to zero. For showing the reference sample, we have used the XRD data of the water atomized micron sized AFN powder (Fig. 1c). The *S* parameter is then calculated according to:

$$S = \frac{(I_s/I_f)_n}{(I_s/I_f)_m} \tag{1}$$

where Is is the intensity of the superlattice reflection peak 100, If is the intensity of the fundamental 110 peak, and n and m represent nanopowder and micron sized powders, respectively. For the AFN sample, the *S* value is calculated as 0.52, which indicates a significant destruction of the long range order in the nanosized composite.

3-2-SEM, TEM, EDS and EDS analysis

The scanning electron microscopy (SEM) images of the as-deposited Ag/Fe$_3$O$_4$ nanocomposite (AFN) show that the particles aggregate into an organized spherical structure, which is characterized by a diameter of 10-20 nm. This type of porous aggregate is characterized by large surface area, which could have potential applications in the areas of catalysis and filtration (Figs. 2a, 2b and 2c).

Energy dispersive spectrum (EDS) for the non-magnetic part of the synthesized Ag/Fe$_3$O$_4$ nanocomposite (AFN) has been shown in Fig. 3. Atomic ratio of Ag/Fe is 7.3, much higher than the ratio (1.3) for the sample synthesized in the presence of polyvinylpyrrolidone (PVP), suggesting that the particles are mainly composed of Ag. Therefore, it is believed that most of the Ag and Fe$_3$O$_4$ primary nanoparticles are separated and cannot gather together to form Ag/Fe$_3$O$_4$ nanocomposite under these circumstances. The signals of carbon, silicon and chlorine arise from the carbon spray, the silicon plate and the reactant Fe$_2$O$_3$.
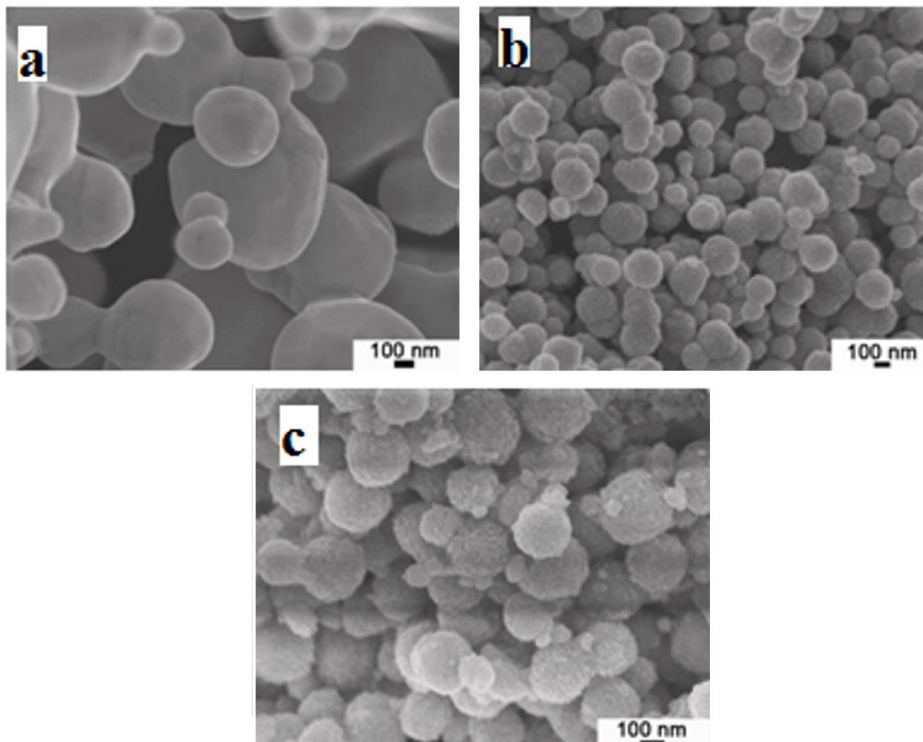
Fig.2. SEM images of the as-prepared Ag (a), Fe_3O_4 (b) particles and the Ag/Fe_3O_4 anocomposite (c) after five cycles of catalytic reaction.
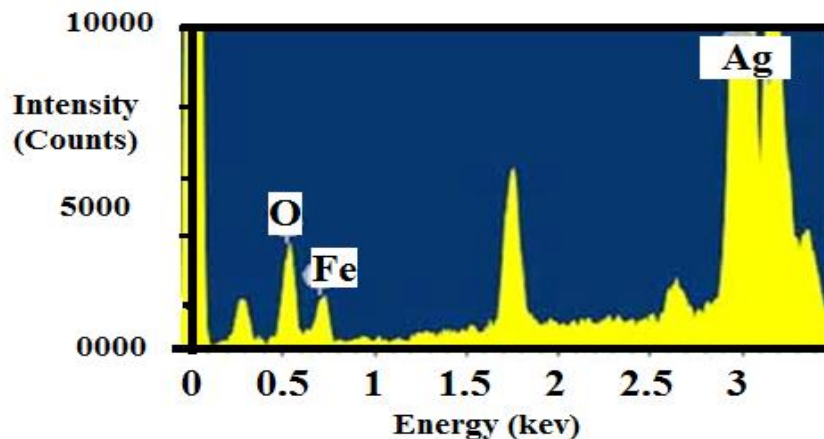
Fig.3. Energy dispersive spectrum (EDS) for the non-magnetic part of the synthesized AFN product.

Fig. 4 displays a transmission electron microscopy (TEM) image of the Ag/Fe_3O_4 nanocomposite (AFN) along with the associated electron diffraction X-ray (EDX) pattern. The observation of multiple rings reveals no preferential orientation within the AFN. The d -spacings calculated from the Electron diffraction (ED) pattern match the d -spacings reported for bulk Ag/Fe_3O_4 nanocomposite (AFN) [58], thus confirming the intermetallic nature of the nanosized AFN powders. The population size distribution calculated from several TEM images shows the average particle diameter to be 15-25 nm.
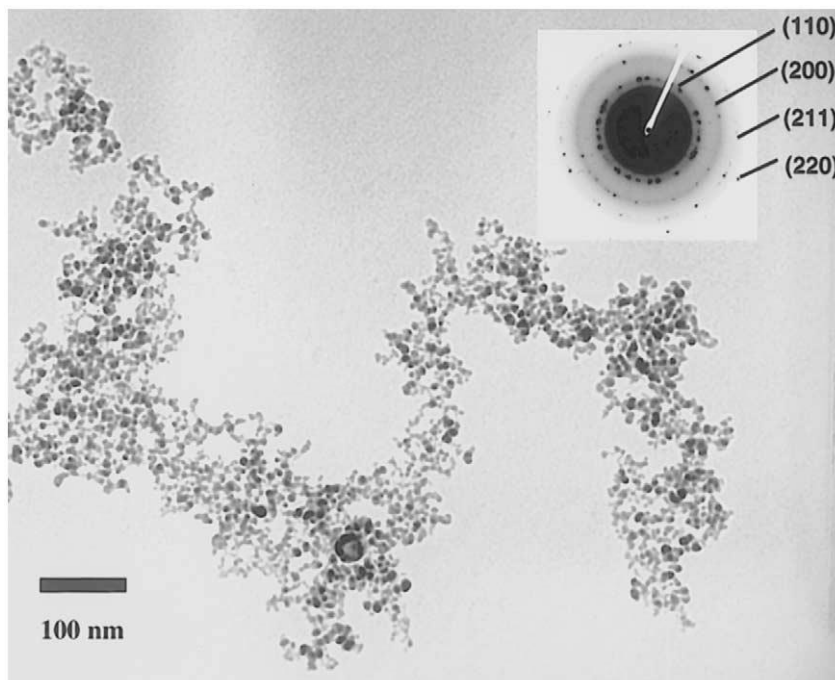
Fig.4. TEM image of the Ag/Fe$_3$O$_4$ nanocomposite (AFN). Insert shows the electron diffraction pattern from the nanoparticles.

A few larger particles which are approximately 40-50 nm in diameter are also observed. The AFN are found to have an amorphous coating surrounding the crystalline core. The coating is approximately 2 nm for the 40 nm particles. Two different approaches were used for characterizing the amorphous coating. First, we carried out an energy dispersive X-ray (EDX) analysis for the nanocomposites during the TEM investigation. The peaks corresponding to emissions from Fe, Ag and O were observed from the electron diffraction X-ray (EDX) spectrum collected by focusing the electron beam into the center of a single 20 nm AFN. On focussing the electron beam closer to the edge of the particle, the electron diffraction X-ray (EDX) spectrum shows an increase in the Fe content over the Ag content and also a significant increase in the amount of oxygen. These changes indicate that the surface of the nanocomposites or the coating is rich in both Ag and oxygen as compared with the center of the particle. Based on the EDX data, the surface coating of the AFN could most likely be iron

oxide or alternatively a spinoidal Ag iron oxide.

Fig.5 shows that the AFN produced by the chemical reaction method is highly charged, and that this phenomenon can be used to generate filaments and tree-like aggregates of the charged nanocomposite. In this case, an electric field (10 -100 V cm-1) is applied across the chamber plates shown in Fig. 5. Following the laser vaporization and the formation of the nanoparticles, it is expected that a mixture of positive and negative charges will accumulate on the particles surfaces, and some of the particles will have net charges. The origin of the charges is believed to be metal ions or electrons generated by the laser vaporization process. The presence of an electric field will induce the polarization of the charges on the surface of the nanoparticles. As a result, the dipole force becomes quite strong near the surface of the particles. Since the nanoparticles can freely rotate within the carrier gas, they can orient their dipoles so that they attract one another, and hence individual particles can stick together by dipole forces.
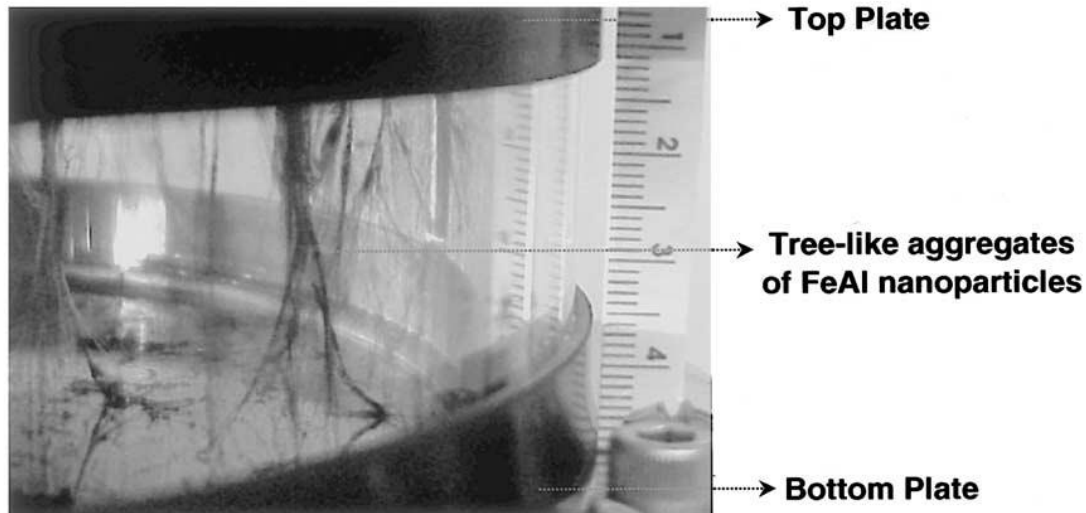
Fig.5. Photographs in the presence of an electric field and tree-like aggregates.

This phenomenon is demonstrated in Fig. 5, which displays a photograph of the laser vaporization followed by controlled condensation (LVCC) chamber with nanoparticle filaments and tree-like aggregates formed in the presence of an electric field. Since no electric shortage occurs when the nanoparticle chains bridge the top and bottom chamber plates, it appears that the nanoparticles are not actually in contact but are apart by small separations enough for dipole forces to be effective. The XRD pattern of the nanoparticles obtained from the chain aggregates is similar to that of the nanoparticles prepared in the absence of the electric field. This indicates that the electric field is only functioning to induce the charge polarization and the electrostatic interaction, and that it has no effect on the chemical composition of the nanoparticles.

It is interesting to note that the growth pattern of the aggregated nanoparticles proceeds from simple chains to filaments to branched filaments, and eventually to complex tree-like aggregates. The generation of intermetallic filaments and fibers of aggregated AFN may have some special applications as fillers (additives) to increase the elastic modulus and tensile strength of polymers such as low strength rubbers.

It is well known that nanoscale particles exhibit a higher microhardness and mechanical strength than micron sized particles as fillers for polymers. This is attributed to the improved bonding between the nanoparticle fillers and the polymer chains.

The Ag/Fe_3O_4 nanocomposite (AFN) obtained is black in color and they possess an apparent low density based on their slow free fall in air. When the powder is approached with a magnet, the particles are instantaneously attracted to the magnet, indicating that the nanoparticles are magnetic at room temperature.

3-3-Stability of the synthesized Ag/Fe_3O_4 nanocomposite (AFN)

Stability of synthesized AFNs was evaluated with termogramitery method at different temperatures after the synthesis of the metal nanocomposites (Fig. 6). It can be seen that the synthesized AFNs are stable in a wider range of temperature from 100 to 600 °C. With increasing the temperature, the weight percentage value of AFNs decreases from 100to 95. It was notable that AFNs found stability in the temperature range of 100 to 600 °C (100 to 95 wt%) and were more stable at 600 °C. The AFNs synthesized via reduction methods are stable under a wide temperature range.
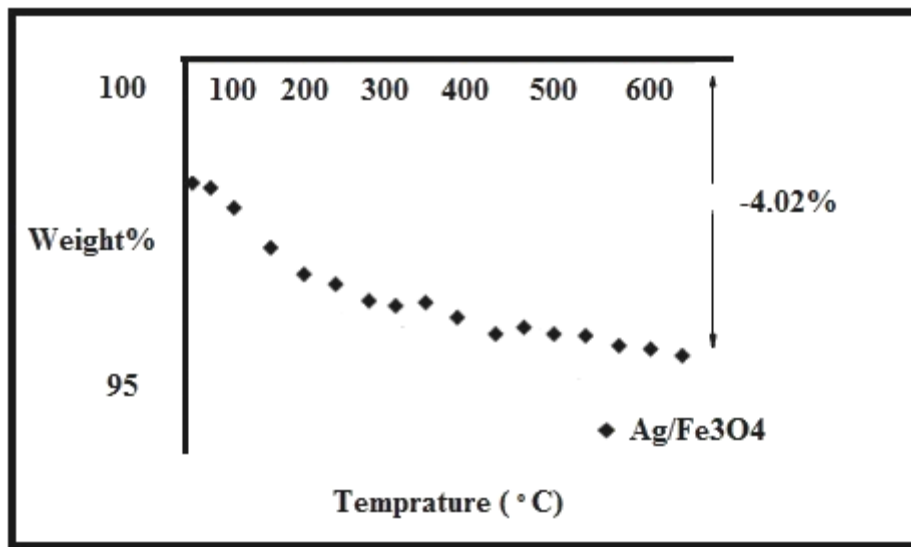
Fig.6. TGA curve in N_2 for Ag/Fe_3O_4 nanocomposite.

3-4-Catalytic activity of Ag/Fe_3O_4 nanocomposite (AFN)

In order to study the catalytic performance of the chemical synthesized Ag/Fe_3O_4 nanocomposite (AFN), the reduction of some aromatic nitro compounds in aqueous solution by NaBH4 was used as the model systems. The catalytic process was monitored by UV–vis spectroscopy as shown in Figs. 7a and 7b. Fig. 7a shows the reduction of 4-nitrophenol (4-NP) to 4-aminophenol (4-AP). 4-NP shows an absorption peak at about 320 with a shoulder at about 400 nm. It can be seen that this peak undergoes a red shift from 320 to 400 nm immediately upon the addition of aqueous solution of NaBH4, corresponding to a significant change in the solution color from light yellow to yellow-green due to the formation of 4-nitrophenolate ion. In the absence of AFN catalyst, the absorption peak at 400 nm remained unaltered for a long duration, indicating that the NaBH4 itself cannot reduce 2-nitrophenolateion without a catalyst. In the presence of AFN catalyst and $NaBH_4$ the 4-NP was reduced, and the intensity of the absorption peak at 400 nm gradually decreased with time and fully disappeared after about 20 min.
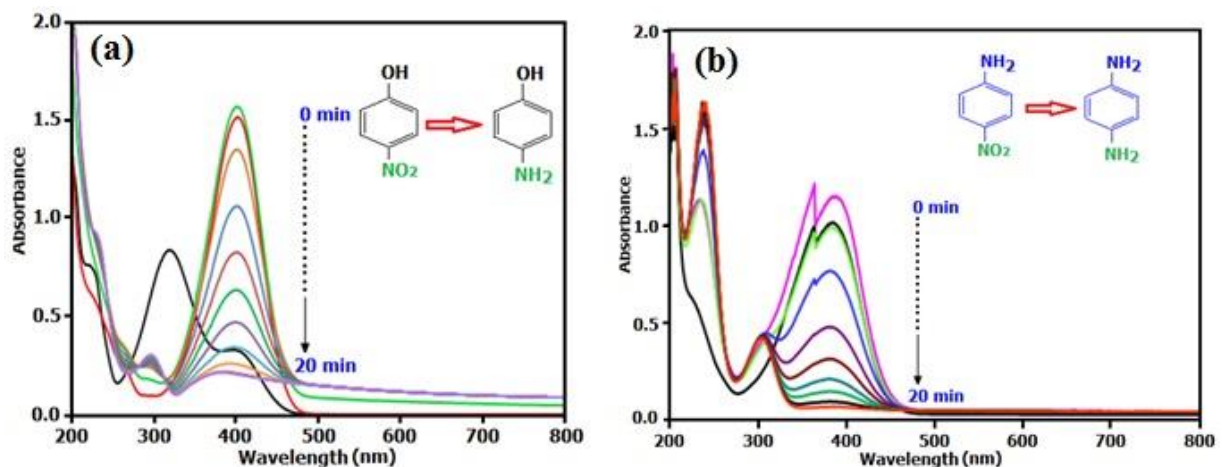
Fig.7. UV–vis spectra of the reduction of nitro compounds with NaBH4 in the presence of Ag/Fe_3O_4 nanocomposite (AFN) as catalyst: (a) 4-nitrophenol and (b) 4-nitroaniline.

At the same time, a new absorption peak appeared at about 298 nm and increased progressively in intensity. This new peak is attributed to the typical absorption of 4-AP. This result suggests that the catalytic reduction of 4-NP exclusively yielded 4-AP, without any other side products. Figs. 7 (a)-(b) show the concentration changes of the two aromatic nitro-compounds with the time in the presence of AFN. The reductive reactions of two aromatic nitro-compounds were finished within 24 min (for 4-NP) and 44 min (for 4-NA), respectively.

Since the reductive reactions were carried out under the same experimental conditions, the above differences of reaction rates were possibly related to the structures of organic compounds.

4-Conclusions

In the present work, Ag/Fe_3O_4 nanocomposite (AFN) was prepared and characterized. The reduction method produces AFN with an average particle size of 10–20 nm and less than 5% of larger particles approximately 40-50 nm. The XRD and EDS measurements confirm that the AFN have the same cubic Ag and Fe structure as the bulk material. Results from EDS and XPS measurements show that the amorphous layer is rich in Fe and oxygen as compared with the core of the particle.

The SEM image of the as-deposited Ag/Fe_3O_4 nanocomposite (AFN) shows the wall thickness of 10 – 20 nm. The AFN generated by the reduction method is highly charged, and can be assembled as tree-like aggregates by applying an electric field across the reaction chamber. The catalytic process of AFN was monitored by UV–vis spectroscopy and shows the reduction of 4-nitrophenol (4-NP) to 4-aminophenol (4-AP). The reduction method can be further developed and optimized to produce a variety of intermetallic nanoparticles for advanced materials applications.

Acknowledgements

References

[1] R. M. German, Powder Metallurgy Science, Metal Powders Industries Federation, 2nd ed., New Jersey, 1997.

[2] F. V. Lenel, Powder Metallurgy Principles and Applications, Metal Powders Industries Federation, 6th ed., New Jersey, 1980.

[3] Yule J. Dunkley, Atomization of Melts for Powder Production and Spray Deposition, Oxford Series on Advanced Manufacturing, 8th ed., Clarendon Press, Oxford, 1994.

[4] M. A. Meyers, K. K. Chawla, Mechanical Metallurgy, 3rd ed., Prentice-Hall, Engelwood Cliffs, NJ, 1984.

[5] H. Hwang, Yeol Lee, K., Yeo, T., W., "Investigation of structural and chemical transitions in copper oxide microstructures produced by combustion waves in a mixture of $CuO–Cu_2O–Cu$ and fuel" Appl. Surf. Sci. Vol. 359, 2015, pp. 931-938.

[6] P. G. Sanders, J. A. Eastman, J. R. Weertman, "Elastic and tensile behavior of nanocrystalline copper and palladium" Acta Mater. Vol. 45, 1997, pp. 4019-4025.

[7] E. Bonetti, L. Pasquini, E. Sampaolesi, "The influence of grain size on the mechanical properties of nanocrystalline aluminium" Nanostruct. Mater. Vol. 9, 1997, pp. 611-614.

[8] X.Y. Qin, X. J. Wu, L.D. Zhang, "The microhardness of nanocrystalline silver" Nanostruct. Mater. Vol. 5, 1995, pp. 101- 110.

[9] Y. Akaltun, M. Aslan, T. Yetim, T. Çayır, A. Çelik, "The effect of wettability on corrosion resistance of oxide films produced by SILAR method on magnesium, aluminum and copper substrates" Surf. Coatings Tech. Vol. 292, 2016, pp. 121-131.

[10] J.C. Rawers, "Effect of heat-treatment on the nanostructure change of W-Cu powder" Nanostruct. Mater. Vol. 11, 1999, pp. 1055-1060.

[11] T. Yinhai, M. Yang, G. Hongyi, J. Li, G. Wang, "A facile approach for fabrication of TiO_2 hierarchical nanostructures and their photocatalytic properties", Colloid. Sur. A: Physicochem. Eng. Aspects Vol. 508, 2016, pp. 184-191.

[12] A., Godon, J. Creus, S. Cohendoz, E. Conforto, X. Feaugas, P. Girault, C. Savall, "Effects of grain orientation on the Hall–Petch relationship in electrodeposited nickel with nanocrystalline grains" Scripta Metall. Mater. Vol. 62, 2004, pp. 403-406.

[13] R. A. Varin, J. Bystrzycki, A. Calka, "Characterization of nanocrystalline Fe–45 at% Al intermetallic powders obtained by controlled ball milling and the influence of annealing" Intermetal. Vol. 7, 1999, pp. 917-930.

[14] H. Mostaan, F. Karimzadeh, M. H. Abbasi, "Synthesis and formation mechanism of nanostructured NbAl3 intermetallic during mechanical alloying and a kinetic study on its formation" Thermochim. Acta. Vol. 529, 2012, pp. 36-44.

[15] L. Yu, S. Yang, H. Wang, Q. Xue, "An investigation of the friction and *and* wear behaviors of micrometer copper" J. Appl. Polym. Sci. Vol. 77, 2000, pp. 2404-2410.

[16] M. A. Barakat, A. M. Al-Ansari, R. Kumar, "Synthesis and characterization of Fe−Al binary oxyhydroxides/ MWCNTs nanocomposite for the removal of Cr (VI) from aqueous solution" .J. Taiwan Inst. Chem. Eng. Vol. 63, 2016, pp. 303-311.

[17] G. Sauthoff, The phase diagram of the binary Fe-Zr system was redetermined by differential. Intermetallics, VCH, Germany, 1995.

[18] N. S. Stoloff , "Iron aluminides: present status and future prospects" Mater. Sci. Eng. A. Vol. 258, 1998, pp. 1-14.

[19] V. K. Sikka, S. C. Deevi, V. K. Sikka, P. J. Maziasz, R. W. Cahn, International Symposium on Nickel and Iron Aluminides: Processing, Properties and Applications, 5th. ed., ASM International Materials. 1997, p. 361.

[20] A. S. Tofik, M. Taddesse Abi, K. T. Tesfahun, G. G. Girma, "Fe–Al binary oxide nanosorbent: Synthesis, characterization and phosphate sorption property" J. Environ. Chem. Engin. Vol. 4, 2016, pp. 2458-2468.

[21] V. K. Sikka, S. Viswanathan, C. G. McKamey, R. Darolia, J. J. Lewandowski, C. T. Liu, P. L. Martin, D. B. Miracle, M. V. Nathal, Structural Intermetallics, The Materials Society, Warrandale PA, 7th ed., 1993, p. 483.

[22] X. Guo, X. Li, Z. Wei, X. Li, L. Niu, "Rapid fabrication and characterization of superhydrophobic tri-dimensional Ni/Al coatings" Appl. Surf. Sci. Vol. 387, 2016, pp. 8-15.

[23] C. G. McKamey, N. S. Stoloff, V. K. Sikka, Physical Metallurgy and Processing of Intermetallic Compounds, Chap- man and Hall, New York, 1996, p. 351.

[24] A. Canakci, F. Erdemir, T. Varol, R. Dalmış, S. Ozkaya, "Effects of a new pre-milling coating process on the formation and properties of an Fe–Al intermetallic coating" Powder Technol. Vol. 268, 2014, pp. 110-117.

[25] S. C. Deevi, "Powder processing of FeAl sheets by roll compaction" Intermetallic. Vol. 8, 2000, pp. 679-685.

[26] H. A. Nalwa, Handbook of Nanostructured Materials and Nanotechnology. Synthesis and Processing, Academic Press, 2nd ed., San Diego, 2000, p. 1.

[27] A. S. Edelstein, R. C. Cammarata, Nanomaterials: Synthesis, Properties and Applications, Institute of Physics Publishing, 2nd ed., Bristol, 1996.

[28] K. Piloj, G.C. Hadijipanyis, R. W. Seigel, Nanophase Materials: Synthesis, Properties and Applications, Kluwer, 3rd ed., London, 1994.

[29] M. S. El-Shall, S. Li, M. A. Duncan, Advances in Metal and Semiconductor Clusters, JAI Press, London, 1998, p.115.

[30] A. Jegan, A. Ramasubbu, S. Saravanan, S. Vasanthkumar, "One-pot synthesis and characterization of biopolymer – Iron Oxide nanocomposite" Int. J. Nano Dimens. Vol. 2, 2011, pp. 105-110.

[31] Ch. Wang, Y. Chen, X. Shang, X. Hou, H. Li, Z. Guo, "Facile synthesis of Ca/Mg/Al/Fe layered double hydroxides using steelmaking slag as raw material" Mater. Lett. Vol. 173, 2016, pp. 115-118.

[32] M. K. Dutta, S. K. Pabi, B. S. Murty, "Phase fields of nickel silicides obtained by mechanical alloying in the nanocrystalline state" J. Appl. Phys. Vol. 87, 2000, pp. 8393-8400.

[33] Y. Shen, W. Gong, B. Zheng, L. Gao, "Ni–Al bimetallic catalysts for preparation of multiwalled carbon nanotubes from polypropylene: Influence of the ratio of Ni/Al" Appl. Catalys. B: Environmen. Vol. 181, 2016, pp. 769-778.

[34] N. Qi, M. Hu, Z. Wang, Z. Lu, "Changsheng XieSynthesis of Al/Fe_3Al core–shell intermetallic nanoparticles by chemical liquid deposition method" Adv. Powder Technol. Vol. 24, 2013, pp. 926-931.

[35] J. Liu, "Cumaraswamy Vipulanandan Effects of Au/Fe and Fe nanoparticles on Serratia bacterial growth and production of biosurfactant" Mater. Sci. Engin. C. Vol. 33, 2013, pp. 3909-3915.

[36] Ch. He, J. Zhang, G. Song, G. Ma, Z. Du, J. Wang, D. Zhao, "Microstructure and mechanical properties of reactive sputtered nanocrystalline (Ti,Al) N films" Thin Solid Films. Vol. 584, 2015, pp. 192-197.

[37] J. A. Haber, J. L. Crane, W. E. Buhro, C. A. Frey, S. M. L. Sastry, J. J. Balbach, M. S. Conradi, "Chemical synthesis of nanocrystalline titanium and nickel aluminides from the metal chlorides" Adv. Mater. Vol. 8,

1996, pp. 163-166.

[38] Ph. Dibandjo, C. Zlotea, R. Gadiou, C. Matei Ghimbeu, F. Cuevas, M. Latroche, E. Leroy, E. Vix-Guterl, "Hydrogen storage in hybrid nanostructured carbon/palladium materials: Influence of particle size and surface" Int. J. Hydrogen Energy. Vol. 38, 2013, pp. 952-965.

[39] H. Y. Sohn, S. PalDey, "Synthesis of ultrafine particles and thin films of Ni$_4$Mo by the vapor-phase hydrogen coreduction of the constituent metal" Metall. Trans. B. Vol. 29, 1998, pp. 457-464.

[40] X. Y. Cheng, W. Q. Liu, Q. Li, "The mechanism of order-induced intrinsic embrittlement in a stoichiometric Ni$_4$Mo alloy by TEM and 3DAP characterization" Mat. Sci. Eng: A. Vol. 486, 2008, pp. 177-182.

[41] K. V. Rajulapati, C. C. Koch, Nanocrystalline Materials: Mechanical Properties. Ref. Module in Mater. Sci. Mater. Eng. 2016, Current as of 28 October 2015.

[42] R. W. Siegel, "Synthesis and Properties of Nanophase Materials" Mater. Sci. Eng. A. Vol. 168,1993, pp.189-197.

[43] B. Huang, W. Xiong, Q. Yang, Z. Yao, G. Zhang, M. Zhang, "Preparation, microstructure and mechanical properties of multicomponent Ni$_3$Al-bonded cermets" Ceramics Int. Vol. 40, 2014, pp. 14073-14081.

[44] K. L. Choy, H. A. Nalwa, Handbook of Nanostructured Materials and Nanotechnology. 1: Synthesis and Processing, Academic Press, 1st Ed, San Diego, 2000.

[45] M. A. S. Sadjadi, B. Sadeghi, M. Meskinfam, K. Zare, J. Azizian, "Synthesis and characterization of Ag/PVA nanorods by chemical reduction method" Physica E: Low-dimensional Systems and Nanostructures. Vol. 40, 2008, pp. 3183-3186.

[46] B. Sadeghi, M. A. S. Sadjadi, R. A. R. Vahdati, "Nanoplates controlled synthesis and catalytic activities of silver nanocrystals" Superlatt. Microstruc. Vol. 46, 2009, pp. 858-863.

[47] B. Sadeghi, M. Jamali, Sh. Kia, A. Amini Nia, S. Ghafari, "Synthesis and characterization of silver nanoparticles for antibacterial activity" Int. J. Nano Dimens. Vol. 1, 2010, pp. 119-124.

[48] B. Sadeghi, F. S. Garmaroudi, M. Hashemi, H. R. Nezhad, A. Nasrollahi, Sima Ardalan, Sahar Ardalan, "Comparison of the antibacterial activity on the nanosilver shapes: nanoparticles, nanorods and nanoplates" Adv. Powder Tech. Vol. 23, 2012, pp. 22-26.

[49] B. Sadeghi, A. Pourahmad, "Synthesis of silver/poly (diallyldimethylammonium chloride) hybrid nanocomposite" Adv. Powder Tech. Vol. 22, 2012, pp. 669-673.

[50] B. Sadeghi, Sh. Ghammamy, Z. Gholipour, M. Ghorchibeigy, A. Amini Nia, "Gold/HPC hybrid nanocomposite constructed with more complete coverage of gold nano-shell" Mic & Nano Lett. Vol. 6, 2011, pp. 209-213.

[51] B. Sadeghi, "Preparation of ZnO/Ag nanocomposite and coating on polymers for anti-infection biomaterial application" Spectrochimica Acta Part A: Molec. Biomolec. Spect. Vol. 118, 2014, pp. 787-792.

[52] B. Sadeghi, M. Meskinfam, "A direct Comparison of nanosilver particles and nanosilver plates for the oxidation of ascorbic acid" Spectrochimica Acta Part A: Molec. Biomolec. Spect. Vol. 97, 2012, pp. 326-328.

[53] B. Sadeghi, "Green synthesis of silver nanoparticles using seed aqueous extract of Olea europaea" Int. J. Nano Dimens. Vol. 5, 2014, pp. 575-581.

[54] B. Sadeghi, A. Rostami, S. S. Momeni, "Facile green synthesis of silver nanoparticles using seed aqueous extract of *Pistacia atlantica* and its antibacterial activity" Spectrochimica Acta Part A: Molec. Biomolec. Spect. Vol. 134, 2015, pp. 326-332.

[55] B. Sadeghi, F. Gholamhoseinpoor., "A study on the stability and green synthesis of silver nanoparticles using *Ziziphora tenuior (Zt)* extract at room temperature" Spectrochimica Acta Part A: Molec. Biomolec. Spect. Vol. 134, 2015, pp. 310-315.

[56] B. Sadeghi, "Zizyphus mauritiana extract-mediated green and rapid synthesis of gold nanoparticles and its antibacterial activity" J. Nanostruct. Chem. Vol. 5, 2015, pp. 265-273.

[57] S. Sadeghi, M. Mohammadzadeh, B. Babakhani, "Green synthesis of gold nanoparticles using *Stevia rebadiauna* leaf extracts: Characterization and their stability" J. Photochem. Photobiol. B. Biology. Vol. 148, 2015, pp. 101-106.

[58] PCPDFWIN X-Ray Database, Version 2.00, (1998) Copyright JCPDS-ICDD.

[59] K. R. Morrison, M. J. Cherukara, K. G. Vishnu, A. Strachan, "Role of atomic variability and mechanical constraints on the martensitic phase transformation of a model disordered shape memory alloy via molecular dynamics" Acta Materialia. Vol. 69, 2014, pp. 30-36.